2013 American Control Conference (ACC)
Washington, DC, USA, June 17-19, 2013

Control-oriented time-varying input-delayed temperature model for SI engine exhaust catalyst

Delphine Bresch-Pietri, Thomas Leroy, Nicolas Petit

***Abstract*— This paper proposes a model for the internal temperature of a SI engine catalyst. The modeling approach is grounded on a one-dimensional distributed parameter model, which is approximated by a time-varying input-delay system whose dynamics parameters (time constant, delay, gains) are obtained through a simple analytic reduction procedure. Following recent works, the distributed heat generation resulting from pollutant conversion is shown here to be equivalent to an inlet temperature entering the system at a virtual front inside the catalyst. The gain of this new input introduces a coupling to account for the conversion efficiency. Relevance of this model is qualitatively supported by experimental data.**

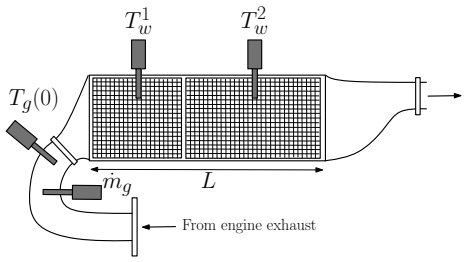

Fig. 1. Experimental catalyst composed of two monoliths. Two sensors permit to measure the wall temperature in the center of each monolith. Test-bench is also equipped with inlet temperature and mass flow sensors.

I. INTRODUCTION

Automotive SI engines are equipped with a Three-Way Catalyst (TWC) located in the exhaust line. This after-treatment device aims at reducing the three major pollutants resulting from the combustion: hydrocarbons HC, carbon monoxide CO and nitrogen oxide NO_x. Yet, conversion efficiency highly depends on the catalyst temperature [8] [9], as presented in Fig. 4. Right after a cold start of the engine, temperatures are too low to activate chemical reactions and the catalyst conversion ratio is poor [17]. Therefore, speed-up of the catalyst warm-up is a point of critical importance to reach high level of pollutant conversion.

Classically, warm-up strategies exploit combustion timing shifting [7], which usually leads to combustion efficiency degradation. Indeed, by appropriately modifying the ignition angle of the mixture, higher exhaust gas temperature can be achieved, leading to a faster heating of the catalyst (monolith). Due to the previously mentioned detrimental effects on combustion, this open-loop technique yields substantial consumption increase. This increase must be limited to its strict minimum. Therefore, it is of prime importance to determine when the catalyst has reached its light-off temperature[1] to obtain a satisfactory compromise between pollutant emissions and consumption. When this light-off temperature is obtained, optimal combustion can be performed and the consumption can simply go back to a standard level.

Determination of the switch time can be achieved from the measurements provided by a commercially embedded temperature sensor located into the cooling system. The thermal behavior of the water cooling system can be indirectly related to the engine and exhaust line temperatures. Yet, this information is relatively uncertain, as other sources of heat can bias it.

An alternative is to rely on models. Some catalyst temperature models have been proposed in the literature. In [10], a mean-value (spatially lumped) model is presented, in which the catalyst temperature follows a first-order dynamics, assuming the temperature inside the wall temperature (i.e. the solid substrate temperature) as spatially homogeneous. This kind of model can be inaccurate since it does not take into account the inherent transport phenomenon and the distributed nature of the catalyst. In particular, it usually leads to an overestimation of the light-off temperature. On the other hand, in [11], [14] or [4], catalyst temperature is represented as Partial Differential Equations (PDE) modeling heat exchange and chemistry inside the monolith, with complex representations of the heat release by chemical reactions. Provided reliable values for all the model parameters are known, these models give very accurate estimation of the light-off temperature, but the induced computational burden discards them from real-time implementations.

In this paper, we propose to use a semi-lumped model of these PDE equations. Following the overture presented in [12], we obtain a first-order input-delay dynamics relating the inlet gas temperature to a punctual wall catalyst temperature. The chemical reactions inside the catalyst are simply represented as a fictitious second temperature front entering the catalyst afar off the physical catalyst inlet. Here, this model is shown to be quite accurate, and of gentle implementation complexity.

The model presented here can be seen as a generalization of [12] to SI engines applications. The main modifications consists in the introduction of the catalyst conversion effi-

D. Bresch-Pietri is with the Department of Mechanical Engineering, MIT, Cambridge, MA 02139 *Email : dbp@mit.edu*

T. Leroy is with the Département Contrôle, Signal et Système in IFP Energies nouvelles, 1-4 Av. du Bois Préau, 92852 Rueil Malmaison, France

N. Petit is with the Centre Automatique et Systèmes, Unité Mathématiques et Systèmes at MINES ParisTech, 60 Bd St Michel, 75272 Paris, France

[1]Defined here as the temperature at which the catalyst becomes more than 90 percent effective.

978-1-4799-0176-0/$31.00 ©2013 AACC

ciency impacting the heat release. This efficiency depends on the output of the model, resulting into an additional coupling which does not tamper with the stability of the model. This model and its use to determine the light-off temperature from experimental data are the main contributions of the paper.

The paper is organized as follows. In Section II, we present the catalyst under consideration in experiments. In Section III, we detail the PDE temperature modeling which is used in Section IV to derive a first-order input-delay model through analytic formula stemming from simple operational calculus. Finally, in Section V, we give some preliminary results of experimental determination of the light-off temperature of the catalyst to stress the relevance of the model.

II. Experimental set-up

The catalyst under consideration in this study is mounted at the outlet of a 2L four-cylinder turbocharged SI engine, downstream the turbine. Fig. 1 presents a scheme of the catalyst under consideration. It is composed of two separated monoliths [18] in charge of oxidizing carbon monoxides and hydrocarbons into carbon dioxide and water, and reducing nitrogen oxides to nitrogen and oxygen[2]. For experimental studies and comparisons, the catalyst has been instrumented with two internal temperature sensors. Such sensors located are not embedded inside any commercial line product. Fig. 2 presents experimental results obtained at test bench during a NEDC (New European Driving Cycle) cycle. Histories of both the exhaust mass flow and the temperature located upstream the catalyst are reported in Fig. 2(a). These quantities are the inputs of the model proposed in this paper. The exhaust mass flow is a fast-varying variable closely related to the engine torque output. The exhaust temperature has a slower dynamics because of the pipes thermal inertia. In Fig. 2(b), both monolith temperatures of Fig. 1 are given[3]. By comparing these two curves between them and against the inlet gas temperature, one can easily see the impact of the catalyst thermal inertia since it deeply slows down the temperature response inside the monoliths. A second important point to notice is the visible very low-pass filter role of the catalyst (see the signals T_w^1 and T_w^2 on Fig. 2(b)). We will account for this in our proposed model simplification.

III. Partial Differential Equation (PDE) Model

We now refer to Fig. 3, where a schematic representation of the monolith is given. Exhaust burned gas enter the monolith at $x=0$ and convective exchange with the wall occur all along the monolith, i.e. for $x=0$ to $x=L$, yielding to inhomogeneously distributed temperature profiles of the gas $T_g(x,t)$ and the catalyst wall $T_w(x,t)$[4].

[2]In the following, the two monoliths are not distinguished. In details, neglecting the conduction inside the wall catalyst yields to the equivalent representation of a unique monolith.

[3]The presented results are obtained by performing optimal combustion during the whole cycle, without warm-up strategy. The duration of the warming phase is therefore longer than a classical one.

[4]On the contrary, the axial conduction in the solid is not important and can be neglected, as underlined in [19], [20]

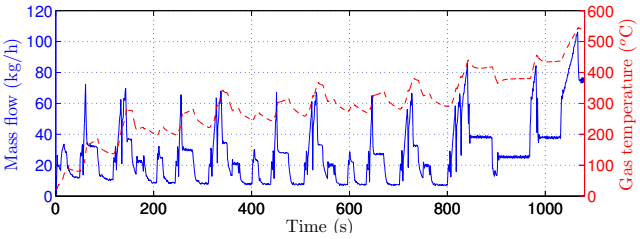

(a) Exhaust gas flow and temperature.

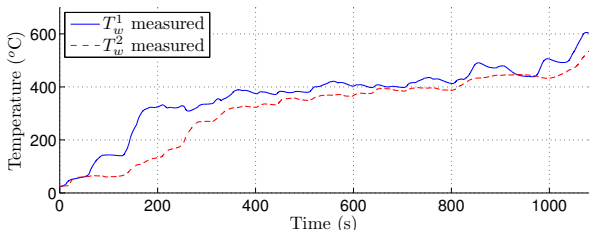

(b) First and second monolith temperature.

Fig. 2. Experimental results on European driving cycle (NEDC).

Here, we consider the following coupled linear infinite dimensional thermal dynamics

$$\begin{cases} \dfrac{\partial T_w}{\partial t}(x,t) = k_1(T_g(x,t)-T_w(x,t)) + \Psi(x,t,T_w(x,t)) & (1) \\ \dot{m}_g \dfrac{\partial T_g}{\partial x}(x,t) = k_2(T_w(x,t)-T_g(x,t)) & (2) \end{cases}$$

where ψ is a distributed time-varying source term, related to the chemical reaction occurring inside the catalyst and the constants $k_1, k_2 > 0$ are defined as

$$k_1 = \frac{h_I P_I}{A_w \rho_w C p_w}, \quad k_2 = \frac{h_I P_I}{C p_g}$$

Such a model is considered for example in [11]. It encompasses the detailed modeling (16)-(17) given in Appendix, provided that a few simplifications are performed:

- conduction ($\lambda_w \partial^2 T_g / \partial x^2$) into the monolith is neglected compared to convection exchanges;
- gas storage is considered as very small compared to the monolith one, i.e. $\rho_g C p_g << \rho_w C p_w$;
- convective exchanges with the atmosphere are neglected compared to the one with the exhaust gas[5].

The source term ψ gathers the sum of the enthalpies of the various reactions taking place inside the catalyst. It can be

[5]This last assumption is only made for sake of simplicity in the following analysis and can easily be relaxed.

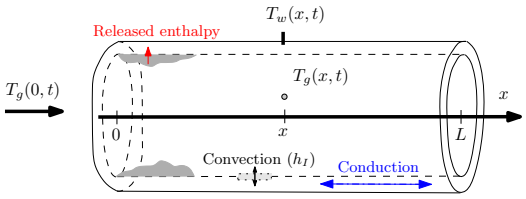

Fig. 3. Schematic view of the distributed profile temperature inside a catalyst jointly with thermal exchanges.

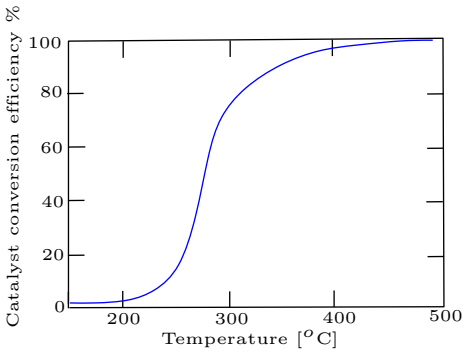

Fig. 4. Conversion efficiency (jointly for CO, HC and NO_x) as a function of temperature for typical catalytic converter (Source : [8]).

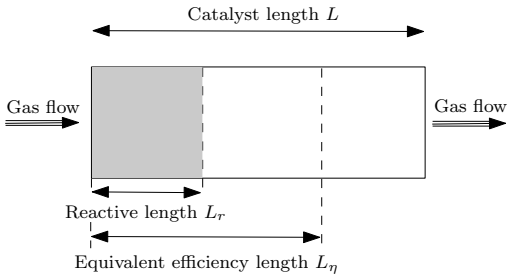

Fig. 5. Schematic view inspired from [12]. The conversion is assumed to take place on an upstream part of the catalyst of length L_r. The temperature used to determine the catalyst efficiency is located at length $L_\eta \leq L$.

effectively represented as

$$\Psi(x,t,T_w) = \begin{cases} \psi(x,t,T_w) & \text{for} \quad 0 \leq x \leq L_r \\ 0 & \text{for} \quad L_r < x \leq L \end{cases}$$

where L_r is the length of the portion of the catalyst where the heat is released. This model is illustrated in Fig. 5 and notations are gathered in Table I. This source term also depends on the wall temperature. This is important to study the light-off process. For moderate temperature, the conversion efficiency highly depends on the wall temperature and this dependence cannot reasonably be neglected.

In this paper, we propose to represent the conversion efficiency of the catalyst as a function of a punctual wall temperature, at a position L_η (potentially varying with aging). Experimental determination of this efficiency was performed and follows the tendency of Fig. 4. In the following, it is called η, considered as a known function, and we focus on the design of a simple model of the wall temperature at L_η[6], handling the potential variability of this position[7].

IV. Approaching the dynamics by an input-delay ordinary differential equation

A. Operational calculus without source term

Before detailing the global model that we propose to use, we focus on the analysis of the "purely thermal" behavior of the PDE model, i.e. without any source term. This case is representative of a temperature interval below $250-300C$, where chemical conversion is almost ineffective.

[6]An effective length L_η was identified as the one of the first monolith.

[7]Yet, in the following, for experimental validation, we also compute wall temperature estimates at other locations.

Symbol	Description	Unit
A_w	Catalyst wall area	m^2
A_g	Catalyst efficient area	m^2
Cp_w	Catalyst wall heat capacity	J/kg/m^3
Cp_g	Gas heat capacity	J/kg/m^3
D	Model delay	s
ΔH_{HC}	Unity enthalpy from HC conversion	J/mol
ΔH_{CO}	Unity enthalpy from CO conversion	J/mol
ΔH_{NOx}	Unity enthalpy from NO_x conversion	J/mol
h_I	Internal convection coefficient	J/K/m^2
h_O	External convection coefficient	J/K/m^2
h_i	Enthalpy of the i^{th} species reaction	J
λ_w	Wall conduction coefficient	J/K/m^2
$\dot{m}_g$	Gas mass flow rate	kg/s
P_I	Internal catalyst perimeter	m
P_O	External catalyst perimeter	m
R_i	Reaction rate of the i^{th} species	-
ρ_w	Catalyst wall volumetric mass	kg/m^3
T_w	Distributed monolith temperature	K
T_w^1	Wall temperature in the middle of the first monolith	K
T_w^2	Wall temperature in the middle of the second monolith	K
T_g	Distributed gas temperature	K
τ	Model time constant	s

TABLE I
NOTATIONS

Claim 1: Assume $\psi = 0$. In the range of low (time domain) frequencies, the distributed parameter model (1)-(2) can be approximated by the following set of first-order delayed equations

$$\forall 0 \leq x \leq L, \quad \tau(x,t)\frac{dT_w(x,t)}{dt} = -T_w(x,t) + T_g(0,t-D(x,t)) \tag{3}$$

with

$$\begin{cases} \tau(x,t) = \dfrac{1}{k_1} + \nu\delta(x,t) & (4) \\ D(x,t) = (1-\nu)\delta(x,t) & (5) \end{cases}$$

where ν is a given constant in $[0,1]$ and δ is defined through the integral equation

$$\int_{t-\delta(x,t)}^{t} \frac{k_1}{k_2}\dot{m}_g(s)ds = x \tag{6}$$

1) Comments: The relation (6) implicitly defines a transport delay through past values of the gas flow rate. It corresponds to a transport phenomenon occurring over a length x with a speed $\frac{k_1}{k_2}\dot{m}_g$ accordingly to a Plug-Flow assumption [16]. This time can be understood as a residence time into the monolith (see [3]). As the two main effects of the gas residence inside the monolith are transport and exchange with the monolith, it can reasonably be separated into a first order dynamics with a pure delay effect. The tuning parameter ν can be determined via dedicated tests and allows this model to qualitatively represent a relatively vast range of catalyst devices.

We now detail this modeling.

2) Formulation of claim 1:

a) Transport delay: By taking a spatial derivative of (1), a time-derivative of (2) and matching terms with (1)-(2), one can obtain the decoupled equations, for all $x \in [0,L]$,

$$\begin{cases} \dot{m}_g(t)\dfrac{\partial^2 T_w}{\partial x \partial t} = -k_2\dfrac{\partial T_w}{\partial t} - k_1\dot{m}_g(t)\dfrac{\partial T_w}{\partial x} \\ \dot{m}_g(t)\dfrac{\partial^2 T_g}{\partial x \partial t} + \ddot{m}_g(t)\dfrac{\partial T_g}{\partial x} = -k_2\dfrac{\partial T_g}{\partial t} - k_1\dot{m}_g(t)\dfrac{\partial T_g}{\partial x} \end{cases}$$

where the first equation defining T_w can be reformulated using a spatial Laplace transform (operational calculus) to get

$$\forall t \geq 0\,, \quad (\dot{m}_g(t)p + k_2)\frac{d\hat{T}_w}{dt} = -k_1\dot{m}_g(t)p\hat{T}_w(p,t)$$

This scalar system can be solved as

$$\hat{T}_w(p,t) = \exp\left(-\left[\int_{t_0}^{t}\frac{k_1\dot{m}_g(s)p}{\dot{m}_g(s)p+k_2}ds\right]\right)\hat{T}_w(p,t_0)$$

where t_0 is such that $t_0 \leq t$.

The catalyst, as is visible from experimental data reported in Fig. 2(b), is relatively non-sensitive to high-frequencies. Consequently, by considering only low-level spatial frequencies (i.e., $\dot{m}_g p << k_2$ for any gas flow $\dot{m}_g$), the term below the integral can be substantially simplified[8]. Rewriting the resulting equation into the usual space domain gives

$$\forall x \in [0,L]\,, \quad T_w(x,t) = T_w\left(x - \left[\int_{t_0}^{t}\frac{k_1}{k_2}\dot{m}_s(s)ds\right], t_0\right)$$

Formally, one can define $\delta(x,t) \geq 0$ such that

$$x - \left[\int_{t-\delta(x,t)}^{t}\frac{k_1}{k_2}\dot{m}_s(s)ds\right] = 0$$

which is equivalent to the implicit integral equation (6). Consequently, the wall temperature at abscissa x is formally delayed by

$$\forall x \in [0,L]\,, \quad T_w(x,t) = T_w(0, t-\delta(x,t)) \tag{7}$$

b) First-order model: From there, it is possible to relate the dynamics under consideration to the gas inlet temperature. Consider for a moment that $\delta(x)$ is constant with respect to time. Then, writing (7) in the time Laplace domain, jointly with (1) for $x = 0$, one directly obtains for all $x \in [0,L]$

$$\hat{T}_w(x,s) = k_1\frac{e^{-\delta(x)s}}{s+k_1}\hat{T}_g(0,s) \tag{8}$$

Finally, following the same steps as previously, it is possible to only consider low frequencies ($s << 1$). By following the elements presented in [15],

$$e^{-\delta(x)s} \approx \frac{e^{-(1-\nu)\delta(x)s}}{\nu\delta(x)s+1}$$

[8]The exact relation between time and spatial frequencies remains to be rigorously explored.

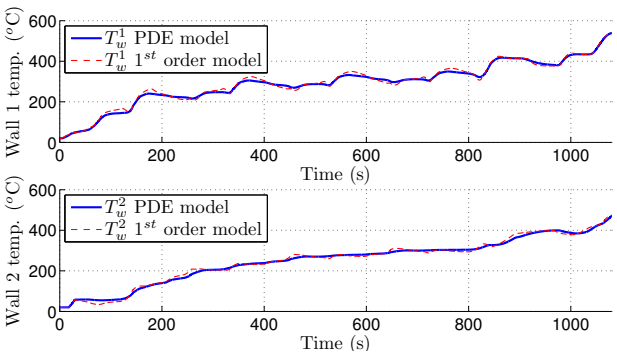

Fig. 6. Simulation comparison between the temperature representation of the model (1)-(2) with $\psi = 0$ and the reduced first-order input-delay model (3)-(6). The inputs of the model are NEDC variations pictured in Fig. 2(a).

with a constant $\nu \in [0,1]$, (8) rewrites for low frequencies as

$$\hat{T}_w(x,s) = \frac{e^{-(1-\nu)\delta(x)s}}{\left(\frac{1}{k_1}+\nu\delta(x)\right)s+1}\hat{T}_g(x,0)$$

By formally generalizing this relation to a time-varying residence time $\delta(x,t)$, one obtains the dynamics formulated in Claim 1.

3) Validation of the reduced model (3)-(6) *using experimental data:* To illustrate Claim 1, simulation results of the temperature inside the wall catalyst at two different locations are pictured in Fig. 6. The two simulation results have been obtained respectively with the distributed parameter model (1)-(2) (with $\psi = 0$, i.e. neglecting the enthalpy flows) and with the proposed simplified dynamics (3)-(6). The inputs used for the two models (gas mass flow rate and gas inlet temperature) are data recorded during a NEDC cycle. They are pictured in Fig. 2(a). In particular, one can observe that the considered gas mass flow rate variations are quite large.

The proposed model was previously calibrated using experimental data for different given operating points, for which the engine was initially cold and requested torque and engine speed were kept constant. In particular, the parameter ν was adjusted during this calibration procedure.

The simulated temperature in Fig. 6 almost perfectly matches the one computed with the PDE model. As these performances are obtained for very demanding external conditions, one can reasonably expect similar behavior on different kinds of driving conditions. For typically encountered input signals, the PDE model is well represented by the model of Claim 1.

Nevertheless, these models cannot completely match experimentally measured data, as the heat released from chemical reactions is neglected. We now investigate this point.

B. Including chemical reactions energy

To account for the source term ψ, we propose to consider the pollutant conversion effects as a second temperature front T_{eq} occurring at virtual position L_r inside the catalyst [9]. This

[9]In details, this fictitious length does not exactly match the physical non-reactive length introduced earlier in Section III. Yet, for sake of simplicity, we assume here that they are identical.

model allows one to exploit the linearity of the dynamics (3)-(6), through a superposition principle, to distinguish the $T_g(0)$ effects from the pollutant conversion effect. This model approach is pictured on Fig. 7.

For steady-state conditions, energy balance for the system can be written as

$$\dot{m}_g Cp_g \underbrace{(T_g(0) - T_g(L))}_{\triangleq T_{eq}} + \eta(T_w(L_\eta)) \sum_{i=1}^{N} \Delta H_i [x_i]_{in} = 0$$

where $[x_i]_{in}$ are the inlet pollutant concentrations. Typically, three main pollutants are considered ($N = 3$), i.e. hydrocarbons (HC), carbon monoxide (CO) and nitrogen oxides (NO_x). They result in three steady-state gains

$$G_{HC} = \eta(T_w(L_\eta)) \frac{\Delta H_{HC}}{\dot{m}_g Cp_g}, \quad G_{CO} = \eta(T_w(L_\eta)) \frac{\Delta H_{CO}}{\dot{m}_g Cp_g}$$
$$\text{and} \quad G_{NO_x} = \eta(T_w(L_\eta)) \frac{\Delta H_{NO_x}}{\dot{m}_g Cp_g}$$

where the unity enthalpy $\Delta H_{HC}, \Delta H_{CO}$ and ΔH_{NO_x} are known constants. These gains are then used to calculate an equivalent temperature

$$T_{eq} = G_{HC}[HC]_{in} + G_{CO}[CO]_{in} + G_{NO_x}[NO_x]_{in} \tag{9}$$

In practice, the pollutant concentrations are not measured but can be effectively estimated, e.g. by look-up tables.

An important point to notice is the appearance of the temperature at length L_η as a parametrization of the conversion efficiency. This yields a coupling represented in Fig. 7 under a closed-loop form.

We summarize this approach by the following claim.

Claim 2: For any source term ψ, the wall catalyst temperature at position L_η can be efficiently represented as

$$T_w(L_\eta) = T_w^{th} + T_w^{\psi} \tag{10}$$

where T_w^{th} satisfies

$$\tau(L_\eta, t) \frac{dT_w^{th}}{dt} = -T_w^{th}(t) + T_g(0, t - D(L_\eta, t)) \tag{11}$$

and T_w^{ψ} satisfies

$$\tau(L_\eta - L_r, t) \frac{dT_w^{\psi}}{dt} = -T_w^{\psi}(t) + T_{eq}(0, t - D(L_\eta - L_r, t)) \tag{12}$$

T_{eq} is defined in (9), the time constant τ and the delay D are defined for $x \in [0, L]$ as

$$\begin{cases} \tau(x,t) = \dfrac{1}{k_1} + \nu\delta(x,t) & (13) \\ D(x,t) = (1-\nu)\delta(x,t) & (14) \end{cases}$$

with ν a given constant in $[0,1]$ and δ defined through the integral equation

$$\int_{t-\delta(x,t)}^{t} \frac{k_1}{k_2} \dot{m}_g(s) ds = x \tag{15}$$

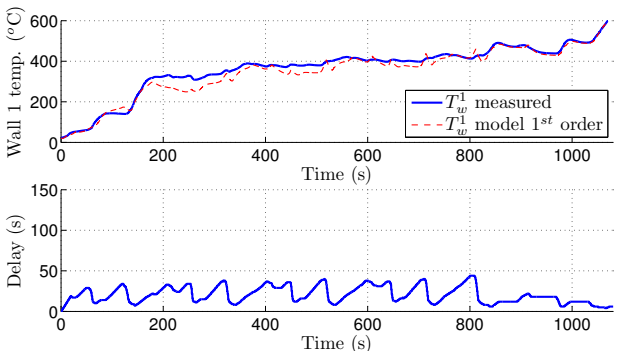

(a) Simulation results for the first-order input-delay model approach, compared to experimental data in the center of the first monolith, and the corresponding delay used in the model.

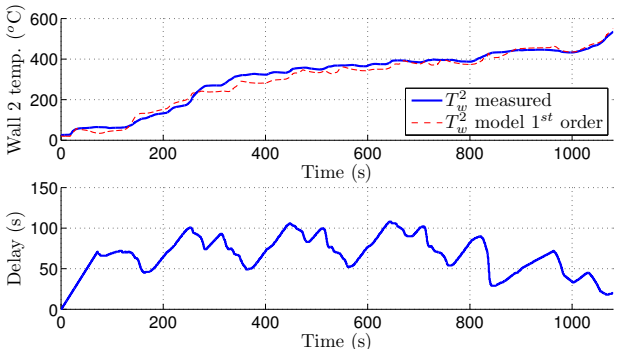

(b) Simulation results for the first-order input-delay model approach, compared to experimental data in the center of the second monolith, and the corresponding delay used in the model.

Fig. 8. Comparison between the proposed model and experimental data at two location inside the monolith.

It is worth noticing that the catalyst temperature at any position $x \in [0, L]$ can also be computed by a similar procedure, provided one has value of the steady-state gains (correspondingly, $T_w(L_\eta, .)$ has to be calculated independently).

C. Validation of the proposed model on experimental data

Simulation results of the wall catalyst temperature at two positions (described in Fig. 1) are provided in Fig. 8 and compared to experimental measurements. These measurements were obtained on a NEDC cycle, with an initially cold catalyst. The tuning parameter is set to $\nu = 0.4$.

One can easily notice that the computed temperatures catch both short-term and long-term variations of the true signals. As previously, it is worth noticing that the inputs corresponding to this NEDC cycle are highly variable and therefore this test case is challenging.

D. Comments about the proposed model

The proposed model is simple enough to be implemented in real-time and provides accurate estimation of the wall catalyst. One clear advantage of the proposed technique that is worth noticing is that it provides insight into the temperature everywhere inside the monolith. A lumped model (or 0D-model) like the one presented in [10] for example, cannot achieve this. Also worth noticing is the fact that aging of the catalyst can be accounted for by updating L_η.

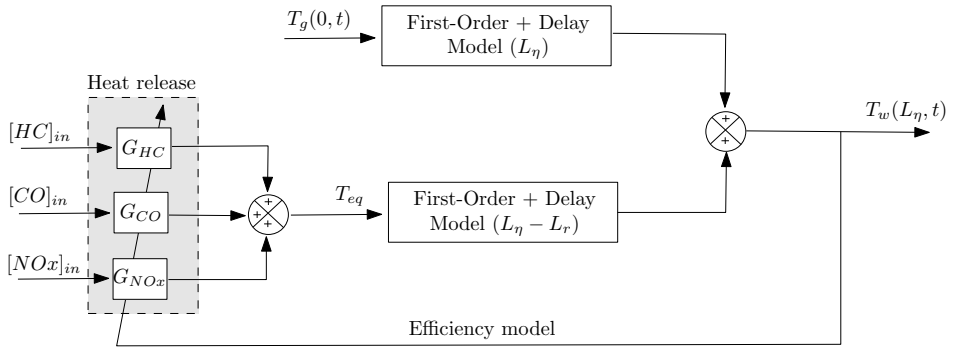

Fig. 7. Proposed catalyst temperature model (10)-(15). The pollutant conversion effects (HC, CO and NO_x) are assimilated to a front of temperature T_{eq} propagating on a virtual length $L_\eta - L_r$, while the gas heating occurs on the complete length L_η. The model is also fed by the gas mass flow rate $\dot{m}_g$ which is not represented here for sake of clarity.

To feed the model, values for various inputs, presented in Fig.7, are necessary: the mass flow rate, the inlet gas temperature and the pollutant emissions upstream of the catalyst.

In practice, the information of the mass flow rate is given by a model already implemented for combustion control purposes (namely, cylinder charge estimation). Further, a certain number of inlet gas temperature models have been proposed in the literature and can be used here if no sensor is available. For example, the interested reader can refer to [6] where a complex 1D model is presented or to [5] for lumped parameter exhaust temperature models.

One direction of future work is the quantitative evaluation of the impact of the use of these models/look-up tables (instead of sensors). In particular, the sensitivity of this model to errors in pollutant emissions would be worth being investigated, as look-up tables computed off-line should be used in practice (preferably with two sets of look-up tables, depending if the engine is cold or warm)

V. Light-off time determination from experimental data

In this section, we use the proposed reduced model to determine the light-off temperature reaching time, i.e. the time when the efficiency of the catalyst is greater than 90 percent. With this aim in view, we consider two sets of experimental data: a NEDC cycle and a FTP one.

For each set, we use the efficiency function calibrated previously, fed with the proposed temperature model at length L_η[10], and compare our computed light-off time with the reference time, determined from downstream pollutant emissions measurements. Results are reported on Table V. One can notice that this determination is quite accurate, but could certainly benefit from a further calibration.

For comparison, on the NEDC cycle, one obtains that the temperature of the cooling system corresponding to light-off is 73^oC. If one would rely on this lagged value to represent the internal catalyst temperature, it would typically result into an overestimation of more than $50s$ on the FTP cycle (Federal Test Procedure).

[10]This length, together with the efficiency function, are here determined off-line using optimization techniques. An hyperbolic tangent function is used to represent the efficiency but can be adjusted online.

	Reference Time	**Reduced model**
Time shifting (NEDC) [s]	350	328
Time shifting (FTP) [s]	190	171

TABLE II

Determination on experimental results of the light-off timing.

Further, one can then schedule in advance the end of the combustion degradation by exploiting the input-delay form of the model (3)-(6) and provide a tailored prediction. Namely, assuming that the external conditions remain similar (i.e., for $s \in [t, t+D(t)]$, $\tau(s) = \tau(t)$), then it is possible to predict the future value of the wall temperature by integrating (3) between t and $t+D(t)$ starting with the current temperature model (see [1] for details regarding this technique). When this predicted temperature achieves the catalyst light-off, optimal combustion can be performed. In details, due to the delayed input, the gas temperature that are already heating the monolith are sufficient to achieve the desired warming. Therefore, combustion timing can be shifted when such a point is achieved.

The use of this prediction technique on the experimental data provides a reference time of $280s$ on the NEDC cycle and of $113s$ on the FTP, which is compliant with the scale of the delay pictured in Fig. 8.

VI. Conclusion

In this paper, a simple first-order input-delay model of the wall catalyst has been presented. Following the works presented in [12] for Diesel engines, the distributed heat generation resulting from pollutant conversion is represented as a second inlet temperature occurring on a virtual front inside the catalyst. These works has been shown to represent well the behavior of SI engine catalysts, via the introduction of a closed-loop additive coupling on the conversion efficiency.

This model suggests interesting control strategies for the light-off. Further, experiments are needed to evaluate these potential merits. Another direction of work is the quantitative

evaluation of the robustness of this model to input estimation errors.

APPENDIX

In this appendix, we provide a more detailed modeling of the thermal exchanges occurring in the catalyst, from which (1)-(2) is a simplification. Following [4], a thermal balance of the gas leads to the equation

$$\rho_g A_g C p_g \frac{\partial T_g}{\partial t} + \dot{m}_g C p_g \frac{\partial T_g}{\partial x} = h_I P_I (T_w(x,t) - T_g(x,t)) \quad (16)$$

where the first term on the left hand side accounts for the gas energy storage, the second one for transport and the right-hand term for convective exchanges. A similar balance for the wall yields

$$\begin{aligned}\rho_w A_w C p_w \frac{\partial T_w}{\partial t} =& \lambda_w \frac{\partial^2 T_w}{\partial x^2} + \sum_{i=1}^{N} R_i h_i + h_I P_I (T_g(x,t) - T_w(x,t)) \\ &+ h_O P_O (T_{amb} - T_w(x,t)) \end{aligned} \quad (17)$$

where the left-hand side still accounts for the energy storage and the right-hand side represents respectively: i) the conduction/diffusion inside the monolith; ii) the enthalpy flow of the N chemical reactions occurring inside the catalyst (mainly, $N = 3$); iii) the exchange respectively with the gas and the atmosphere.

One can notice that, following [12], no transport occurs in the (solid) wall. In more details, a mass balance of the species in presence can be established. The species concentrations inside the monolith are necessary to determine the reaction terms R_i in the enthalpy flows. Two additional equations per species are also necessary (one for the gas and one for the monolith, see [2] [13]).

ACKNOWLEDGMENT

The authors are thankful to Olivier Lepreux for fruitful discussions and advice and to Sopheaktra Kim, ENSTA ParisTech undergraduate student, who carried out substantial model developments during an internship.

REFERENCES

[1] Z. Artstein. Linear systems with delayed controls: a reduction. *IEEE Transactions on Automatic Control*, 27(4):869–879, 1982.

[2] SF Benjamin and CA Roberts. Automotive catalyst warm-up to light-off by pulsating engine exhaust. *International Journal of Engine Research*, 5(2):125–147, 2004.

[3] PV Danckwerts. Continuous flow systems: distribution of residence times. *Chemical Engineering Science*, 2(1):1–13, 1953.

[4] C. Depcik and D. Assanis. One-dimensional automotive catalyst modeling. *Progress in energy and combustion science*, 31(4):308–369, 2005.

[5] L. Eriksson. Mean value models for exhaust system temperatures. In *Proc. of the Society of Automotive Engineering World Congress*, number 2002-01-0374, 2005.

[6] H. Fu, X. Chen, I. Shilling, and S. Richardson. A one-dimensional model for heat transfer in engine exhaust systems. In *Proc. of the Society of Automotive Engineering World Congress*, number 2005-01-0696, 2005.

[7] L. Guzzella and C. H. Onder. *Introduction to modeling and control of internal combustion engine systems*. Springer Verlag, 2010.

[8] J. B. Heywood. *Internal combustion engine fundamentals*. McGraw-Hill New York, 1988.

[9] U. Kiencke and L. Nielsen. *Automotive control systems*. Springer-Verlag, Berlin, 2000.

[10] D. Kum, H. Peng, and N. K. Bucknor. Optimal energy and catalyst temperature management of plug-in hybrid electric vehicles for minimum fuel consumption and tail-pipe emissions. *IEEE Transactions on Control Systems Technology*, (99), 1999.

[11] P. M. Laing, M. D. Shane, S. Son, A. A. Adamczyk, and P. Li. A simplified approach to modeling exhaust system emissions: SIMTWC. *SAE paper*, -:01–3476, 1999.

[12] O. Lepreux. *Model-based temperature control of a Diesel oxidation catalyst*. PhD thesis, MINES Paristech, 2010.

[13] L. Olsson and B. Andersson. Kinetic modelling in automotive catalysis. *Topics in catalysis*, 28(1):89–98, 2004.

[14] A. Onorati, G. D'Errico, and G. Ferrari. 1D fluid dynamic modeling of unsteady reacting flows in the exhaust system with catalytic converter for SI engines. In *Proc. of the Society of Automotive Engineering World Congress*, number 2000-01-0210, 2000.

[15] L. Pekar and E. Kureckova. Rational approximations for time-delay systems: case studies. In *Proceedings of the 13th WSEAS international conference on Mathematical and computational methods in science and engineering*, pages 217–222. World Scientific and Engineering Academy and Society (WSEAS), 2011.

[16] R. H. Perry, D. W. Green, and J. O. Maloney. *Perry's chemical engineers' handbook*, volume 7. McGraw-Hill New York, 1984.

[17] C. P. Please, P. S. Hagan, and D. W. Schwendeman. Light-off behavior of catalytic converters. *SIAM Journal on Applied Mathematics*, 54(1):72–92, 1994.

[18] K. Ramanathan, D. H. West, and V. Balakotaiah. Optimal design of catalytic converters for minimizing cold-start emissions. *Catalysis today*, 98(3):357–373, 2004.

[19] J. Vardi and W. F. Biller. Thermal behavior of exhaust gas catalytic convertor. *Industrial & Engineering Chemistry Process Design and Development*, 7(1):83–90, 1968.

[20] L. C. Young and B. A. Finlayson. Mathematical models of the monolith catalytic converter. *AIChE Journal*, 22(2):343–353, 1976.